Characterization of Carbon-Containing Aerosolized Drugs Using Laser-Induced Breakdown Spectroscopy

DIBYENDU MUKHERJEE and MENG-DAWN CHENG*

Environmental Sciences Division, Oak Ridge National Laboratory, Oak Ridge, Tennessee 37831

Aerosolized drug delivery methods have increasingly become popular for pharmaceutical applications. This is mainly due to their ease of application and the more recent advancements incorporating nano-sized generation of particles that find deeper penetration routes and more efficient administration of the drug to specific target organs. Their effectiveness heavily relies on the uniformity of the chemical composition of these aerosolized drugs. Thus, it calls for a real-time on-line analytical tool that can accurately characterize the chemical constituents of the drug powder particles generated to ensure a stringent quality control. We present laser-induced breakdown spectroscopy (LIBS) for the first time as an efficient analytical tool to carry out on-line quantitative chemical characterization of aerosolized drugs. We used three different carbon based aerosolized drugs, namely L-ascorbic acid 2-phosphate sesquimagnesium salt hydrate ($C_6H_9Mg_{1.5}O_9P{\cdot}xH_2O$), Iron(II) L-ascorbate ($C_{12}H_{14}FeO_{12}$), and DL-pantothenic acid hemicalcium salt ($C_9H_{16}NO_5{\cdot}0.5Ca$) for our quantitative LIBS studies here. Our results show that LIBS can effectively estimate the quantitative ratios of carbon to various trace elements for each of these drugs, thereby enabling on-line unique characterization of individual aerosolized drugs. The quantitative LIBS technique predicted the [C]/[Mg], [C]/[Fe], and [C]/[Ca] ratios as 4.02 ± 0.76, 12.42 ± 2.36, and 18.47 ± 4.39 for each of the above aerosolized drugs, respectively. Within error limits, we find these ratios in good agreement with the respective stoichiometric values of 4, 12, and 18 corresponding to the drugs above. Thus, the work demonstrated the utility and validity of LIBS in accurate on-line identification of drug powders during real-time manufacturing processes.

Index Headings: **Laser-induced breakdown spectroscopy; LIBS; Aerosol; Drugs; Elements.**

INTRODUCTION

In recent years, laser-induced breakdown spectroscopy (LIBS) has gained increasing interest among popular analytical techniques for real-time chemical characterization of solids, gases, or aerosols.[1] The main reason for such interest stems from the inherent nature of LIBS that makes it simple and fast, as well as requiring minimal sample preparation for most on-line chemical analysis applications. Commonly, LIBS has already been extensively used for elemental analysis of steel,[2] alloys,[3] rubber,[4] trace metals,[5,6] and toxic emission[7,8] detections or even in art preservation efforts.[9] From the environmental and health perspectives, recently there has been a strong drive to demonstrate the efficacy of LIBS for detection and analysis of atmospheric aerosols,[10,11] particularly relevant for carbonaceous aerosols[12] and ambient bio-aerosols.[13,14] With such diverse applications of LIBS, it has potential in the pharmaceutical sector as a real-time on-line chemical analysis technique to ensure strict quality control and reliability of their manufacturing processes. Yet, only a few recent works have tried to completely characterize the LIBS technique in terms of its suitability for pharmaceutical applications, especially for its use as a quantitative analytical tool for on-line elemental analysis of drugs manufactured in aerosolized form.

Traditionally, high-performance liquid chromatography (HPLC) has been the most commonly used technique for chemical analysis of pharmaceutical products. However, this technique has its own limitations since it requires lengthy sample preparation and collection and hence is not suitable for on-line real-time chemical characterization of drugs at the production site. Recently, Gupta, et al.[15] attempted to outline an on-line analytical HPLC procedure enabling quantitation of compounds directly injected from metered dose inhalers (MDI). However, the method did not allow for real-time quantitative elemental analysis of aerosolized drugs during the manufacturing process. Other analytical techniques such as inductively coupled plasma optical emission spectroscopy or flame and graphite furnace atomic absorption spectroscopy call for lengthy sample dissolution or digestion steps. Such steps call for elaborate off-line effort in these methods, which in turn also results in the turnaround time being significantly long.[16] Clearly there is a need for rapid on-line quantitative analytical techniques in the pharmaceutical sector.

Among the other on-line analytical techniques available for monitoring of manufacturing processes, near-infrared (NIR) spectroscopy is the most well-established.[16] A number of works have already demonstrated the suitability of NIR spectroscopy for various analytical measurements of pharmaceutical products, including quantitative characterization of powder blend uniformity,[17,18] coating processes during drug manufacturing,[19] and real-time particle size determination of pharmaceutical nanoparticles.[20] However, these indicate a severe lack of real-time quantitative elemental analysis of aerosolized drugs produced on-the-fly during pharmaceutical manufacturing processes.

A few works have demonstrated the use of LIBS for quantitative analysis of pharmaceutical products in tablet form[21,29,30] by presenting schemes to improve the analytical performance of LIBS for rapid on-line quantitative chemical composition assessment of pharmaceutical products. Other works include application of LIBS for rapid on-line analysis of coating thickness and uniformity,[22] magnesium stearate content[31] during batch manufacturing of pharmaceutical tablets, and comparison of scanning electron microscopy and LIBS as solid-phase elemental analysis techniques requiring no sample preparations.[23] But these works have mostly been restricted to the analysis of bulk drugs in solid tablet form. In recent years, Mukherjee et al.[24] developed a LIBS experimental methodology that allowed for

Received 11 September 2007; accepted 5 February 2008.

* Author to whom correspondence should be sent. E-mail: chengmd@ornl.gov.

0003-7028/08/6205-0554$2.00/0

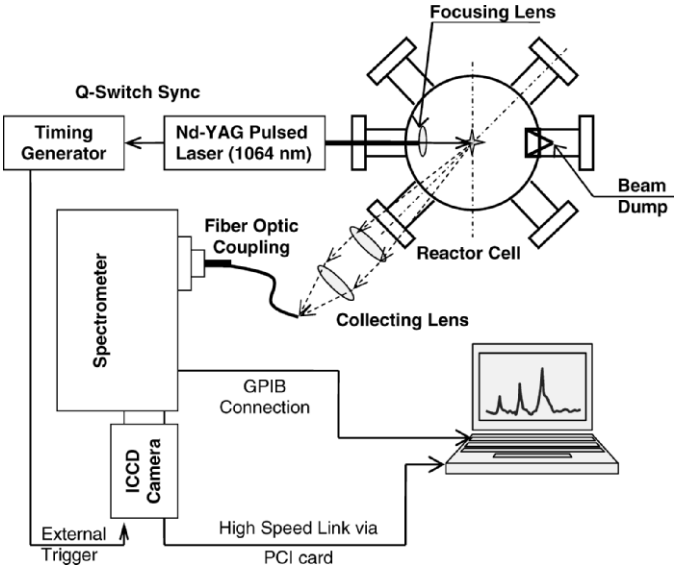

FIG. 1. Schematic of the LIBS experimental setup.

real-time quantitative characterization of multi-component aerosols using an internal calibration scheme without the need for any sample preparation or external material standards. Such research efforts indicate new opportunities for LIBS in quantitative chemical analysis of aerosols and throw light on the future of quantitative LIBS in pharmaceutical applications.

Very few attempts have tried to establish an on-line chemical characterization technique for air-borne drug powders, which in many cases is the primary form of the drugs in the initial stages of their manufacturing process. Also, most pulmonary drugs or inhalers are in the dry powder or aerosolized form. To the best of our knowledge, the only work citing LIBS in the chemical analysis of pharmaceutical products in powdered form ends up evaluating the relative merits of near-infrared (NIR) spectroscopy and LIBS in terms of their statistical accuracy, precision, and selectivity when applied to the determination of magnesium stearate contents in pharmaceutical powders and solid dosage forms.[16] However, it does not extract any quantitative information regarding the relative elemental composition analysis from the LIBS signal of the studied drugs.

Recently we demonstrated the viability of LIBS for quantitative chemical analysis of carbon-containing aerosolized powders.[12] The goal of the present work is to further extend our studies to the applications of LIBS methodology for chemical analysis of carbon-containing aerosolized drugs by establishing the relative elemental ratios of carbon to various trace elements in different drugs. Such analysis would essentially enable unique characterization of individual drugs based on their chemical make-up. For our studies here, we have used three different aerosolized vitamin products, namely L-ascorbic acid 2-phosphate sesquimagnesium salt hydrate (LAA), Iron(II) L-ascorbate (ILA), and DL-pantothenic acid hemicalcium salt (DLP). For the sake of convenience we shall refer to the drugs as LAA, ILA, and DLP, respectively, from here on. The choice of these products was based on their wide range of carbon and different trace element contents. Also, their non-toxic properties made the experimental setup and safety precautions easier to handle. Our goal here would be to establish the relative ratios of carbon to Mg, Fe, and Ca in each of the respective powdered drugs from the LIBS spectral data analysis and compare the experimentally obtained ratios with the expected stoichiometric values from the known drug formula. The comparison is intended to establish the credential of the quantitative LIBS technique for real-time monitoring of drug powders.

EXPERIMENTAL

Optical Setup. The LIBS experimental system is illustrated in the schematic in Fig. 1. The laser-induced plasma is created with a Q-switched Nd:YAG laser ($\lambda = 1064$ nm; Make: New Wave Research; Model: Tempest-10) of 10 Hz repetition rate operated at an energy of 200 mJ/pulse and a pulse width of 4 ns. The beam is focused with a 25 mm focal length fused silica plano-convex lens (diameter, 25 mm) to provide an estimated fluence of approximately 10–15 GW/cm^2 at the focal point. The subsequent breakdown at the focal point creates a micro-plasma of 1–2 mm^3 volume within which the excitation temperatures might reach up to 10 000–15 000 K. The aerosol flow exits a 0.635 cm tapered nozzle positioned approximately 1 mm right above the plasma breakdown point at the center of the six-arm reactor cell.

The plasma fluorescence is collected in the direction of a 45 degree angle to the incoming focused laser beam, which was found to collect the maximum signal intensity from the plasma plume. The light was collected and collimated by a 200 mm focal length plano-convex lens and was re-focused with a 50 mm focal length plano-convex lens to the tip of a fiber-optic collector coupled to the entrance slit of a 0.5 m 1200 grooves/mm grating Czerny–Turner spectrometer (Make: Acton Research Corp.; Model: SpectraPro 500i). The slit width for all experimental runs was kept at around 70 μm for optimal signal intensity and spectral line widths. The dispersed spectra are recorded at the exit focal plane of the spectrometer with a time-gated intensified charge-coupled device (ICCD) detector array (1024 × 1024 CCD) with an effective linear dispersion of approximately 0.014 nm/pixel (Make: Andor Technology; Model: DH534-18U-03). The time gating was synchronized with the laser Q-switch and controlled via a digital timing generator (Make: Stanford Research Systems; Model: DG535).

Aerosolized Drug Delivery Setup. The aerosol flow setup consisted of an in-house-built dry powder dispersion system as shown in Fig. 2. A simple single-stage ejector pump was used to create a vacuum level of around 40.6 to 47.4 kPa with a high positive air pressure line of 40 kPa. The ejector pump was used to transfer the powder from the tube at a uniform rate while a low air flow rate of around 3–5 L min^{-1} was used to agitate and help deliver the powder via the vacuum suction line into the center of the six-arm reactor cell where the aerosols encounter the laser beam and undergo breakdown. The entire powder dispersion system is placed in a shaker, which prevents the powder from settling down at the bottom of the tube. The agitator flow meter was used to vary the delivery flow rate of the powder in air via the suction line marked as Q_s (L min^{-1}of air) in Fig. 2, which in turn regulated the mass concentrations for the powder delivered into the reactor cell. Particle size distribution data for all three powdered drugs were collected using an aerodynamic particle sizer (APS) (Make: TSI; Model: 3320).

As discussed in our earlier work,[12] the powder delivery system allowed for four different delivery flow rates of $Q_s =$ 3.5, 4.2, 4.6, and 5.6 L min^{-1} of air to vary the mass concentrations of powder delivered within a range such that it

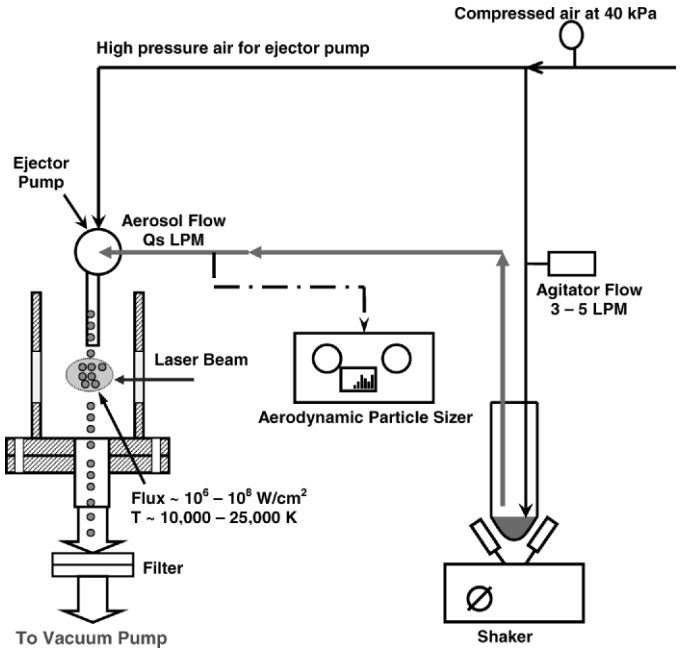

FIG. 2. Schematic of the aerosol line setup.

covered a wide range while allowing a uniform and stable delivery rate for a long enough time to allow sufficient spectral data collection. In the present work, we ran all our experiments for the delivery rate of $Q_s = 3.5$ L min^{-1} of air since it provided the lowest aerosol mass loading and a uniform delivery rate over 2–3 minutes to collect all the spectral data needed for our analysis. The particle size distribution obtained for this delivery rate indicated a median peak diameter of 1 μm, with most particles being in the size range less than 0.7 μm (as indicated below in the Results and Discussion section). This resulted in aerosol mass loadings that were low enough to not cause any major interference from wavelength-specific mass-loading-induced plasma matrix effects, the details of which can be found in our earlier work.[12]

Materials and Samples.. Three different carbon-based powdered vitamin drugs with different carbon contents and trace elements such as iron, calcium, and magnesium were chosen for all the quantitative LIBS experiments here. The products used were: (1) L-ascorbic acid 2-phosphate sesquimagnesium salt hydrate, ≥95% purity (Molecular formula: $C_6H_6Mg_{1.5}O_9P{\cdot}xH_2O$; CAS#: 113170-55-1; Product No.: A8960) with a molecular weight of 289.54 AMU (anhydrous basis); (2) Iron(II) L-ascorbate, ≥90% (titration) purity (Molecular formula: $C_{12}H_{14}FeO_{12}$; CAS#: 24808-52-4; Product No.: A0207) with molecular weight of 406.08 AMU; and (3) DL-pantothenic acid hemicalcium salt, ≥97% purity (Molecular formula: $C_9H_{16}NO_5{\cdot}0.5Ca$; CAS#: 63409-48-3; Product No.: P9153) with molecular weight of 238 AMU. All drugs were Sigma-Aldrich make and their detailed material safety data-sheets were obtained from the Sigma-Aldrich website.[25] The particular choice of these drugs was based upon their wide range of carbon contents and different trace elements (Mg, Fe, and Ca) that were uniquely associated with each of the drugs and were sensitive to LIBS detection. Also, material data sheets confirmed these drugs to be non-toxic and chemically docile.

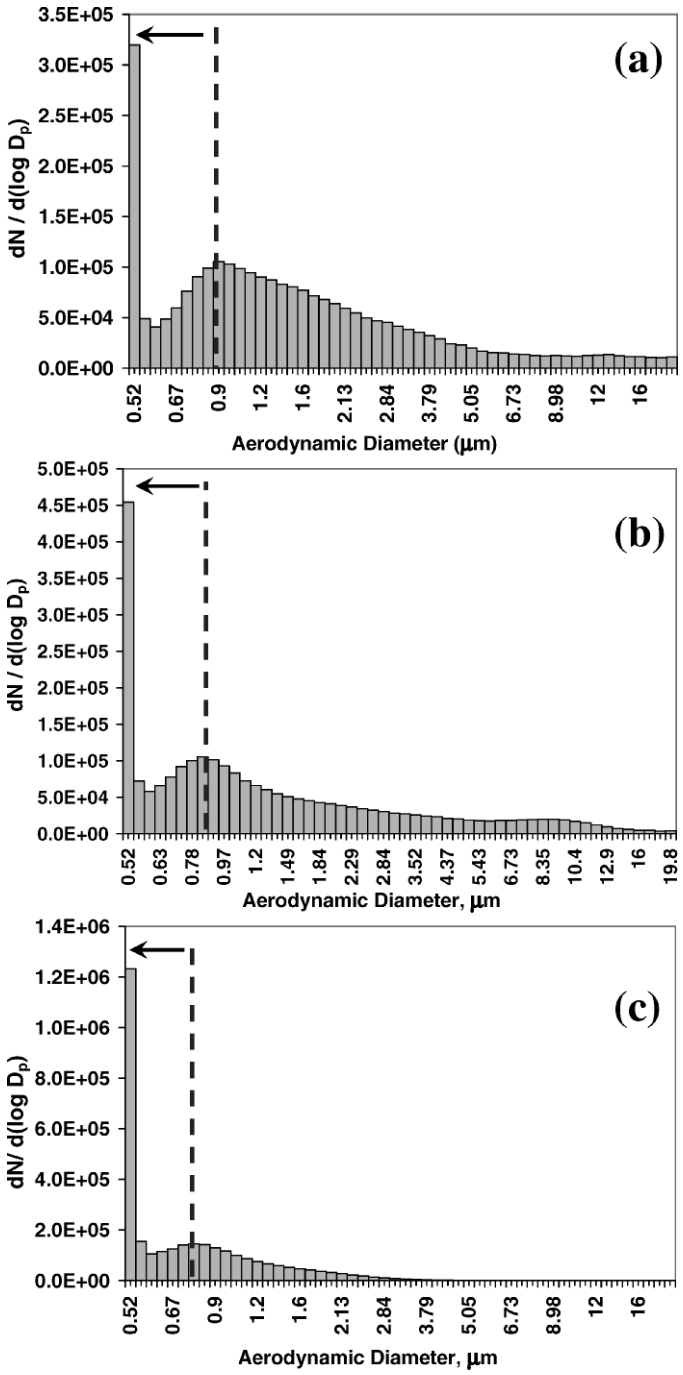

FIG. 3 Particle size distributions for (**a**) ILA, (**b**) LAA, and (**c**) DLP powdered drugs. The dotted line indicates the median diameter (mm), while the arrow points to the largest particle number concentration in the smaller size ranges (<700 nm).

RESULTS AND DISCUSSION

Particle Size Distribution. Our preliminary experimental data consisted of collecting particle size distributions (PSD) for the three drugs under study. Figures 3a, 3b, and 3c indicate the sample PSD for ILA ($C_{12}H_{14}FeO_{12}$), LAA ($C_6H_9Mg_{1.5}O_9P{\cdot}xH_2O$), and DLP ($C_9H_{16}NO_5{\cdot}0.5Ca$), respectively. As seen from the figures, all three aerosolized drugs had an average median diameter around 1 μm, while the distributions had the maximum particle concentrations in the bin of 0.7 μm and smaller size region. In the case of the PSD

TABLE I. Atomic spectral database[26] for the C I, Mg I, Fe I, and Ca I transition lines used for the quantitative elemental characterization of each of the drugs LAA, ILA, and DLP, respectively.

Species	Wavelength (nm)	Transition probability A_{ki} (s^{-1})	g_k	g_i	E_k (eV)	E_i (eV)
C I	247.856	3.40×10^{07}	3	1	7.684766	2.684011
Mg I	285.2127	4.91×10^{08}	3	1	4.3458026	0.0000000
Fe I	404.5813	8.63×10^{07}	9	9	4.5485043	1.4848637
Ca I	422.673	2.18×10^{08}	3	1	2.9325118	0.0000000

for ILA (Fig. 3a), a large number concentration of particles was found below 0.9 μm, with the highest concentrations being lumped into the 0.5 μm bin size. Similar distributions of maximum particle concentrations in the size range bins below 0.5 μm for LAA and DLP were also found. In the case of LAA (Fig. 3b) and DLP (Fig. 3c), maximum particle concentrations were found in the size range below the peak median diameter centered on 0.8 μm and 0.78 μm, respectively. These clearly indicate the abundance of particles in the size domain smaller than 0.7 μm, thereby ensuring the LIBS sampling of these particles to be significantly higher than that for the 10 μm diameter particles. This in turn ensured lesser interference from mass-loading-induced plasma matrix effects anticipated from a wide bi-modal distribution having large concentrations of particle sizes above 1 μm, as seen in our earlier study.[12]

Experimental Methodology. The experimental data and subsequent chemical analysis for the quantitative estimation of elemental ratios by LIBS are based on the methodology described in detail in our earlier works.[12,24] As a brief overview, the methodology entails collecting the LIBS spectra for the respective neutral transition lines of the elemental species of interest, which in the present study were namely carbon (C I) and trace elements, magnesium (Mg I), iron (Fe I), and calcium (Ca I), corresponding to the three drugs LAA, ILA, and DLP, respectively. In the present experiment, the neutral transition lines of C I (247.8 nm), Mg I (285.2 nm), Fe I (404.6 nm), and Ca I (422.7 nm) were selected for all spectral data collected following the initiation of the laser-induced plasma dissociating the three drugs under study. The choice of the C I (247.8 nm) line has already been cited in our earlier work on carbonaceous aerosols,[12] and those for the trace elements were based on their relative strengths, accuracies, and transition probabilities as listed by the NIST Atomic Database.[26] Spectral details for the C I (247.8 nm), Mg I (285.2 nm), Fe I (404.6 nm), and Ca I (422.7 nm) transition lines have been listed in Table I.

The optimal gate delay for the C I (247.8 nm) line was known to be around 3.5 μs from our earlier LIBS experiment on carbonaceous aerosols.[12] The optimal gate delays for Mg I (285.2 nm), Fe I (404.6 nm), and Ca I (422.7 nm) were found to be around 10, 13, and 29 μs, respectively, as estimated from the time evolution of each of the neutral emission lines from the LIBS spectral data collected for the drugs LAA, ILA, and DLP, respectively. The effective emission intensities, I_{em}, of C I and Mg I, Fe I, and Ca I lines were estimated in the form of signal-to-noise ratio (S/N) from the background-subtracted LIBS data collected for each of the respective drugs. The choice of S/N ratio as the effective I_{em} for all the species emission lines collected in this study ensured uniformity of the experimental data across all LIBS spectra collected, as well as nullified any artifacts arising out of background fluctuations.

TABLE II. Atomic spectral database[26] for the different Mg I, Fe I, and Ca I transition lines used for plasma temperature calculations and species emission lines used as internal calibration standards for the LIBS analysis of each of the drugs LAA, ILA, and DLP.

Species	Wavelength (nm)	Transition probability A_{ki} (s^{-1})	g_k	g_i	E_k (eV)	E_i (eV)
Mg I transition lines used in LAA analysis						
Mg I	309.298	3.74×10^{07}	5	3	6.7189877	2.7115918
Mg I	309.689	4.96×10^{07}	7	5	6.7189830	2.7166397
Mg I	382.936	8.99×10^{07}	3	1	5.9459170	2.7091048
Mg I	383.230	1.21×10^{08}	5	3	5.9459132	2.7115918
Mg I	383.829	1.61×10^{08}	7	5	5.9459154	2.7166397
Mg I	516.732	1.13×10^{07}	3	1	5.1078267	2.7091048
Mg I	517.268	3.37×10^{07}	3	3	5.1078267	2.7115918
Mg I	518.360	5.61×10^{07}	3	5	5.1078267	2.7166397
Fe I transition lines used in ILA analysis						
Fe I	357.00970	6.77×10^{07}	11	9	4.3864622	0.9146016
Fe I	358.1190	1.02×10^{08}	13	11	4.3200980	0.8589955
Fe I	381.584	1.30×10^{08}	7	9	4.7331399	1.4848637
Fe I	382.0425	6.68×10^{07}	9	11	4.1033730	0.8589955
Fe I	382.588	5.98×10^{07}	7	9	4.1543532	0.9146016
Fe I	385.9911	9.70×10^{06}	9	9	3.2111889	0.0000000
Ca I transition lines used in DLP analysis						
Ca I	457.855	1.76×10^{07}	5	3	5.2284398	2.5212631
Ca I	458.14	2.09×10^{07}	7	5	5.2284825	2.5229865
Ca I	458.587	2.29×10^{07}	9	7	5.2285405	2.5256819
Ca I	504.162	3.30×10^{07}	3	5	5.1675381	2.7090092
Ca I	643.907	5.30×10^{07}	9	7	4.4506467	2.5256819
Species emission lines used as internal calibration standard						
O I	777.194	3.69×10^{07}	7	5	10.740931	9.1460906
Ca I	430.774	1.99×10^{08}	1	3	4.763168	1.8858073
Mg I	518.36042	5.61×10^{07}	3	5	5.1078267	2.7166397

Here, S/N ratio implied the ratio of peak intensity at species emission wavelength to the root mean square value of the noise, where the noise was calculated by considering 40 pixels along the baseline adjacent to the analyte peak. For all spectral data analysis in this paper, the C I, Mg I, Fe I, and Ca I emission lines collected at their respective gate delays were averaged over 6 to 7 shots comprising 100 accumulations per shot.

As also described in our earlier work,[12,24] under the assumption of local thermodynamic equilibrium (LTE), plasma excitation temperatures are estimated from the slope ($-1/T_{exc}$) of the linear fit to the Boltzmann plot of $\ln(I_{em}\lambda_{ki}/g_kA_{ki})$ versus normalized upper state energies, (E_k/k_B), for a series of strong emission lines with well-spread energy levels.[27] In the present study, for each of the drugs LAA, ILA, and DLP, 6 to 8 transition lines for the respective trace elements (Mg I, Fe I, and Ca I) were used to generate the linear Boltzmann plots. The excitation temperatures from these plots were estimated at the respective gate delays of 3.5 μs for C I data analysis and 10, 13, and 29 μs for data analysis of each of the species emission lines of Mg I, Fe I, and Ca I. An advantage of the presence of trace elements such as Mg, Fe, and Ca in the respective drugs is the abundance of multiple strong neutral transition lines of Mg I, Fe I, and Ca I that one can choose from the laser-induced plasma emissions to construct the linear Boltzmann plots. As discussed in our earlier work,[24] the assumption of LTE for the validity of the Boltzmann plots holds true since all the emission lines are collected beyond 1 μs after plasma initiation. The spectral details[26] for all the strong emission lines of Mg I, Fe I, and Ca I that had a wide spread of energy levels are tabulated in Table II and were used for plasma temperature calculations for the drugs LAA, ILA, and DLP, respectively.

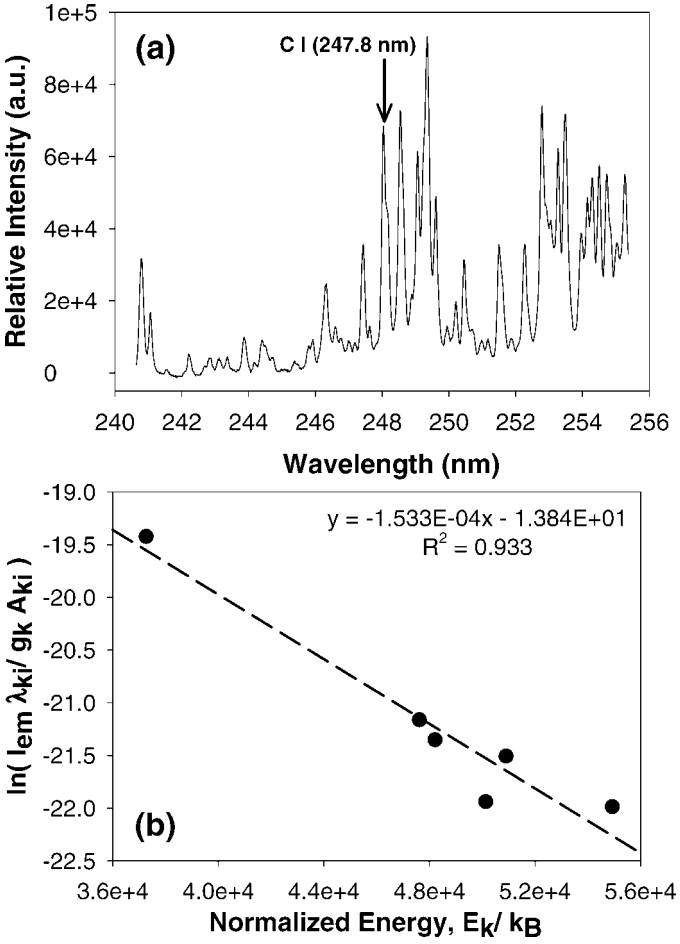

FIG. 4. (**a**) Spectral signature of the C I (247.8 nm) transition line at a gate delay of 3.5 μs and a gate width of 10 μs and (**b**) the corresponding linear Boltzmann plot (regression coefficient of $R^2 \sim 0.933$) with Fe I transition lines (listed in Table II for ILA analysis) used for calculation of $T_{exc} = -1/\text{Slope} = 6522 \pm 872$ K at delay time = 3.5 μs.

Upon collection of all spectral data comprising the relative emission intensities of species transition lines of C I (247.8 nm), Mg I (285.2 nm), Fe I (404.6 nm), and Ca I (422.7 nm) and the plasma excitation temperatures at the respective gate delays, we proceeded to calculate species population densities. Under the assumption of LTE, the relative population densities of all the species of interest (C I, Mg I, Fe I, and Ca I) from the samples injected into the plasma were calculated based on the Maxwell–Boltzmann equation:[28]

$$I_{em} = A_{ki} h \nu_{ki} N_i \frac{g_k}{g_i} \exp\left(-\frac{\Delta E_{ki}}{k_B T_{exc}}\right) \quad (1)$$

where A_{ki} is Einstein's transition probability for the given transitions; ν_{ki} is the frequency of the transition; g_k and g_i are the respective statistical weights for upper state k and lower state i; ΔE_{ki} is the energy difference in Joules between the k and i states; and h and k_B are Planck's and Boltzmann's constants, respectively. The respective plasma excitation temperature at given gate delays is defined as T_{exc}, while N_i is the number density of each species at the lower states at a given time. In the present study, the number densities shall be referred to as N_i^{XI} (where X refers to the different species such as C, Mg, Fe, and Ca).

In line with our earlier work[12,24] developing the quantitative LIBS methodology, we used abundant species emission lines in the plasma as the internal calibration standards for all quantitative estimations of atomic species concentrations calculated from the collected emission intensities (I_{em}) and plasma temperatures (T_{exc}) via the Maxwell–Boltzmann (M-B) relationship given in Eq. 1. Using Eq. 1 the species concentrations, N_i^{Calib}, calculated by using abundant species emission line data collected for identical experimental setups and at specific gate delays, were used to normalize all the relative species population densities of C I, Mg I, Fe I, and Ca I estimated at the respective gate delays for each of the drugs. Table II also lists the abundant species lines of O I (777.2 nm), Ca I (430.8 nm), and Mg I (518.4 nm) used in different cases as the internal calibration standard in this work. The choice of these lines for the different cases studied here are discussed in detail below. The internal calibration technique nullifies the artifacts arising due to optical/experimental setup or time-specific plasma characteristics that affect the transition lines of the species of interest. Finally, with this normalization procedure we obtain the estimated quantitative elemental ratios of [C]/[X] (where X refers to the different species like C, Mg, Fe, and Ca) as:

$$\frac{[C]}{[X]} = \frac{[N_i^{CI}/N_i^{Calib}]_{@GD=3.5\,\mu sec}}{[N_i^{XI}/N_i^{Calib}]_{@GD=10,13,29\,\mu sec}} \quad (2)$$

Drug Analysis. The above-mentioned methodology was carried out on the LIBS data collected subsequently for each of the drugs LAA, ILA, and DLP to estimate the quantitative elemental ratios of [C]/[Mg], [C]/[Fe], and [C]/[Ca], respectively.

Laser-induced breakdown spectroscopy plasma emission lines for C I (247.8 nm) and Fe I (404.6 nm) were collected from the breakdown of aerosolized ILA powders dispersed into the laser-induced plasma plume inside the reactor cell, as described earlier in the Experimental Setup section. Figures 4a and 5a show the typical emission line profiles of C I (247.8 nm) and Fe I (404.6 nm) collected at respective gate delays of 3.5 μs and 13 μs, with a gate width of 10 μs. Due to the existence of a relatively large number of strong Fe I transition lines spread all over the UV-visible spectrum, Fig. 4a indicates the presence of multiple Fe I emission lines next to the C I (247.8 nm), but fortunately, as marked in Fig. 4a, we could uniquely identify the C I (247.8 nm) line since it did not interfere with any of the Fe I transition lines. I_{em} for both the emission lines indicated in Figs. 4a and 5a were estimated from the S/N ratio as described earlier.

It is true that for the case of iron-containing drug powders we saw a significant presence of Fe I lines at 247.98, 248.33, 248.81, and 249.1 nm wavelengths, as indicated in Fig. 4a. However, with the spectral resolution of the spectrometer used, these lines could be easily separated from the C I (247.86 nm) line and hence did not cause any interference in our work. Fe II lines at 247.856 nm and 247.84 nm do not interfere with the carbon line because they decay rapidly and make negligible contributions at the delay time of 3.5 microseconds chosen for the C I lines.[28]

Figures 4b and 5b show the corresponding linear Boltzmann plots for the five Fe I transition lines listed in Table II and used for the plasma excitation temperature, T_{exc}, calculations at the respective time delays of 3.5 μs and 13 μs for the quantitative LIBS analysis of C I and Fe I species concentrations. The regression coefficients of $R^2 \sim 0.93$ and 0.95 indicate a good linear fit for the Boltzmann plots in Figs. 4b and 5b, respectively. Plasma excitation temperatures T_{exc} estimated

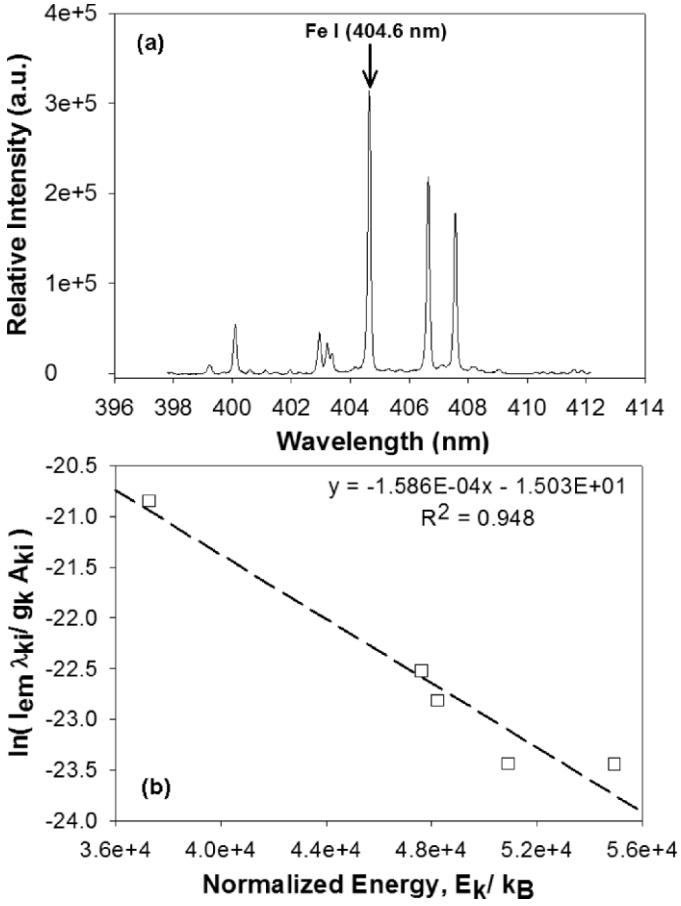

FIG. 5. (**a**) Spectral signature of the Fe I (404.6 nm) transition line at a gate delay of 13 μs and a gate width of 10 μs and (**b**) the corresponding linear Boltzmann plot (regression coefficient of $R^2 \sim 0.948$) with Fe I transition lines (listed in Table II for ILA analysis) used for calculation of $T_{exc} = -1/\text{Slope} = 6306 \pm 849$ K at delay time = 13 μs.

from the slope of the linear fits ($-1/T_{exc}$) in Figs. 4b and 5b were found to be 6522 ± 872 K and 6306 ± 849 K, respectively. The uncertainties were estimated from the regression analysis of the linear fits at the 95% confidence interval. In this case, we also collected the O I (777.2 nm) emission line at the respective gate delays of 3.5 μs and 13 μs to be used for our internal calibration technique, as described before. Species population densities N_i^{CI} and N_i^{FeI} were calculated from Eq. 1 using the respective I_{em} values of the transition lines and the corresponding T_{exc} at the respective time delays. Similarly, the population density of oxygen used as our internal calibration standard in this case, i.e., here $N_i^{Calib} = N_i^{OI}$, was estimated from Eq. 1 using the data for the O I (777.2 nm) line. Upon normalization of N_i^{CI} and N_i^{FeI} population densities with N_i^{OI} as per our methodology discussed above, the quantitative elemental ratio of [C]/[Fe] was calculated as

$$\frac{[C]}{[Fe]} = \frac{[N_i^{CI}/N_i^{OI}]_{@GD=3.5\,\mu sec}}{[N_i^{FeI}/N_i^{OI}]_{@GD=13\,\mu sec}} \cong 12.42 \pm 2.36 \qquad (3)$$

Here the uncertainty in the data was estimated from the error propagation for the statistical uncertainties in the S/N ratio due to signal fluctuations and that in T_{exc} from the uncertainties in the linear fit. The estimation was in good

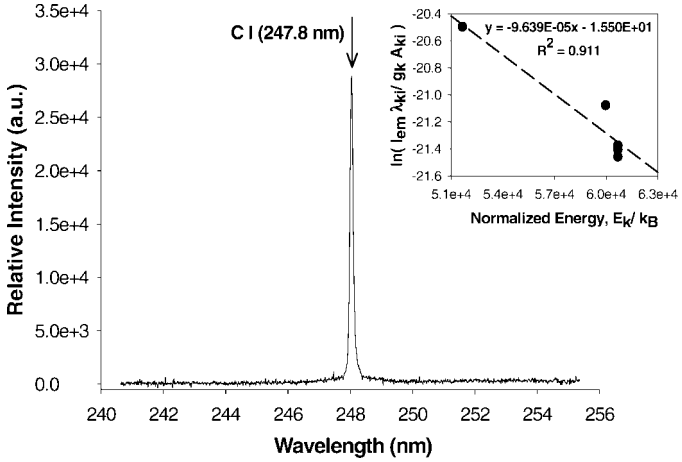

FIG. 6. Spectral signature of the C I (247.8 nm) transition line at a gate delay of 3.5 μs collected from breakdown of DLP powders. (**Inset**) The corresponding linear Boltzmann plot (regression coefficient of $R^2 \sim 0.911$) with Ca I transition lines (listed in Table II for DLP analysis) used for the calculation of $T_{exc} = -1/\text{Slope} = 10374 \pm 1877$ K at delay time = 3.5 μs.

agreement with the expected stoichiometry from the molecular formula, i.e., [C]/[Fe] = 12. This encouraged us to continue this study on the other drugs.

Similar studies were carried out with the other aerosolized drugs, LAA and DLP, as well. In the case of DLP, the time-resolved spectral emission profile for the Ca I (422.7 nm) transition line indicated the optimal gate delay to be 29 μs. The mean emission line for C I (247.8 nm) averaged over 700 shots at the known delay time of 3.5 μs has been plotted in Fig. 6. Similarly, the mean emission line for Ca I (422.7 nm) at 29 μs delay time has been plotted in Fig. 7. From these, the S/N ratio information was extracted for the effective emission intensity data, I_{em}, of each of the C I and Ca I lines. The inset plots in Figs. 6 and 7 indicate the linear fits to the corresponding Boltzmann plots created in this case at the respective gate delays of 3.5 μs and 29 μs for the five strong emission lines of Ca I indicated earlier in Table II. The regression coefficients of $R^2 \sim 0.91$ at the earlier gate delay times of 3.5 μs and $R^2 \sim 0.93$

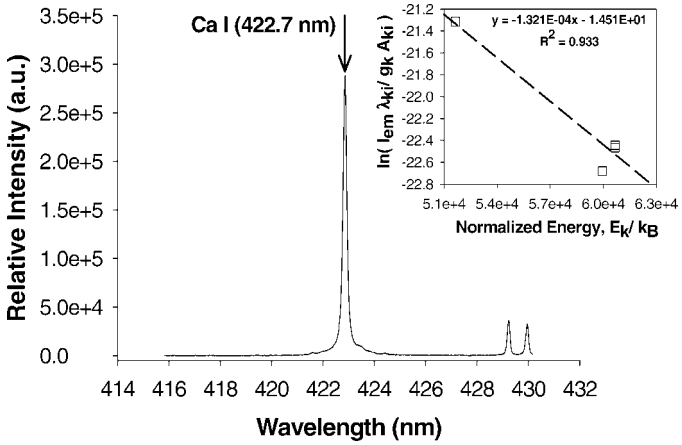

FIG. 7. Spectral signature of the Ca I (422.7 nm) transition line at a gate delay of 29 μs collected from breakdown of DLP powders. (**Inset**) The corresponding linear Boltzmann plot (regression coefficient of $R^2 \sim 0.933$) with Ca I transition lines (listed in Table II for DLP analysis) used for the calculation of $T_{exc} = -1/\text{Slope} = 7569 \pm 1167$ K at delay time = 29 μs.

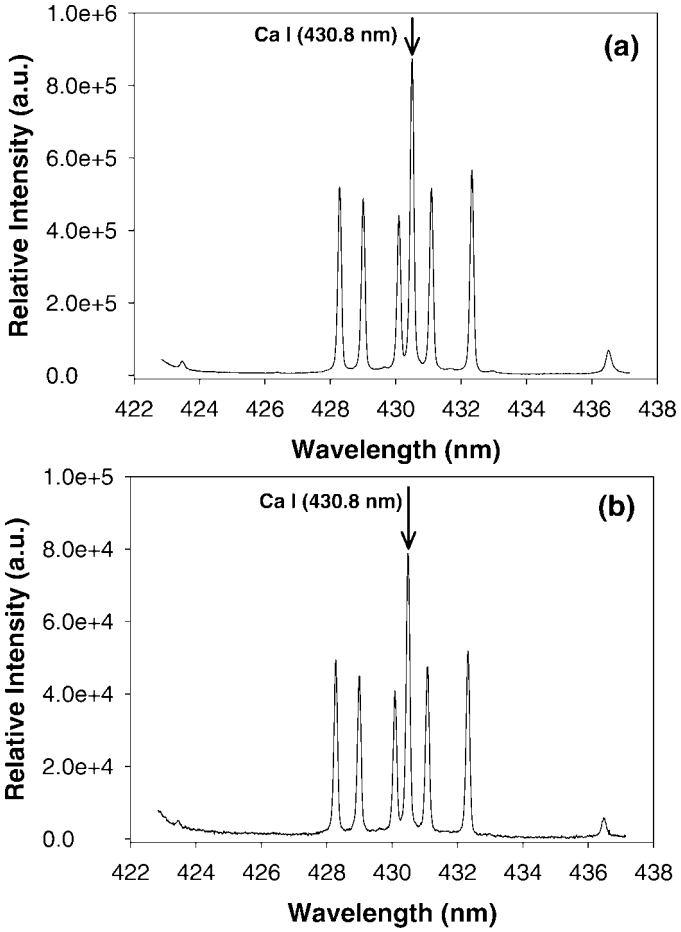

FIG. 8. Typical spectral signatures of the Ca I (430.8 nm) transition line used as the internal calibration standard at the gate delays of (**a**) 3.5 μs and (**b**) 29 μs.

at 29 μs delay time, as indicated in Figs. 6 and 7, respectively, also indicate good linear fits for the plots. Plasma excitation temperatures calculated at the given delay times from the slope of the linear fits resulted in $T_{exc} = 10374 \pm 1877$ K and 7569 ± 1167 K, respectively. In this case, we noticed relatively large uncertainties in plasma temperature calculations from the respective linear Boltzmann plots at gate delay times of 3.5 μs and 29 μs, which could have stemmed from the lack of strong Ca I lines distributed over a wide range of energy levels.

This could be one of the potential limiting factors of LIBS for quantitative chemical analysis, although the problem can be circumvented by the choice of a substantial number of emission lines averaged over a large number of data for generating the linear Boltzmann plots such that the statistical errors are smoothened out. However, this also implies a tradeoff between time and efficiency, both being critical in the face of a real-time chemical analysis scenario. In the present work, time and supply of sufficient chemical samples being the constraining factors, statistical accuracy was relatively compromised in exchange for developing a fast on-line chemical analysis method. Finally, knowing the I_{em} for the C I and Ca I lines and the T_{exc} at gate delay times of 3.5 μs and 29 μs, respectively, we could calculate the species population densities similar to the methodology described in the earlier study of ILA powders.

In this case, the optimal gate delay time for the Ca I (422.7 nm) line being 29 μs, the plasma was in the later stages of its evolution. Hence, it started emitting the molecular lines that

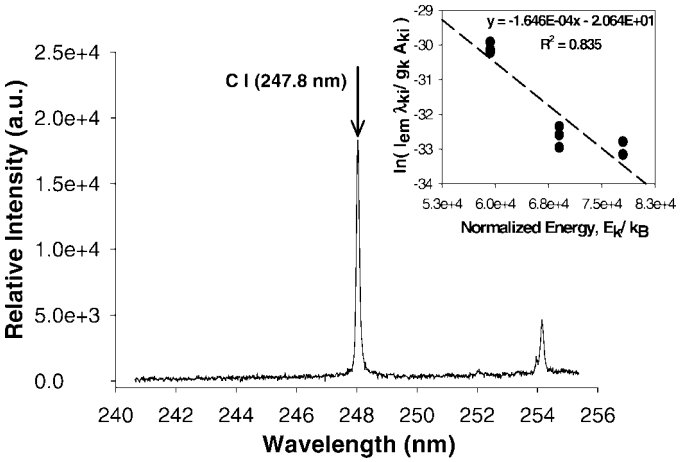

FIG. 9. Spectral signature of the C I (247.8 nm) transition line at a gate delay of 3.5 μs collected from breakdown of LAA powders. (**Inset**) The corresponding linear Boltzmann plot (regression coefficient of $R^2 \sim 0.835$) with Mg I transition lines (listed in Table II for LAA analysis) used for the calculation of $T_{exc} = -1/\text{Slope} = 6076 \pm 1102$ K at delay time = 3.5 μs.

interfered with the atomic transition lines and made it difficult for us to acquire any O I lines, which usually start decaying quickly after about 15–20 μs delay time. Thus, the choice of the O I (777.2 nm) line was no longer suitable as the internal calibration standard. But one has to bear in mind that by normalizing the species relative population densities with the population density of a bulk species in the plasma, the internal calibration technique essentially nullifies any artifact in the LIBS spectral data arising out of the specific experimental/optical setup, such as the spectrometer and camera slit width and specific optical alignments or temporal evolution of plasma volume. Thus, for an identical experimental setup, any abundant emission line acquired from the plasma plume at the specific gate delay of interest can be effectively used in the internal calibration technique to normalize the spectral data collected for the specific species of interest.

In the absence of the O I (777.2 nm) line in the present case, we resorted to the Ca I (430.8 nm) strong neutral transition line of calcium as our internal calibration standard. Typical mean emission line profiles for the Ca I (430.8 nm) transition line collected at gate delays of 3.5 μs and 29 μs and shown in Figs. 8a and 8b, respectively, indicate the presence of a persistently strong emission line of Ca I (430.8 nm) even at the 29 μs time stamp. The species population densities of $N_i^{\text{CaI(430.8nm)}}$ calculated from the S/N ratio of the Ca I (430.8 nm) emission line at the respective gate delay times of 3.5 μs and 29 μs were subsequently used to normalize the species population densities N_i^{CI} and N_i^{CaI}, respectively, as shown in Eq. 2 earlier. Again, the quantitative elemental ratio of [C]/[Ca] in this case was estimated to be 18.47 ± 4.39, in excellent agreement with the value of 18 expected from the molecular formula of DLP.

Finally, we also carried out a similar set of experiments and spectral data analysis on magnesium-bearing LAA powdered drugs. Time-resolved spectral data collected for the chosen Mg I (285.2 nm) emission line indicated the optimal gate delay to be 10 μs. Similar to the earlier cases, neutral transition lines of C I (247.8 nm) and Mg I (285.2 nm) averaged over 700 shots and collected at 3.5 μs and 10 μs are shown in Figs. 9 and 10, respectively. In each case the emission intensity, I_{em} was estimated from the respective S/N ratio for each of the C I and

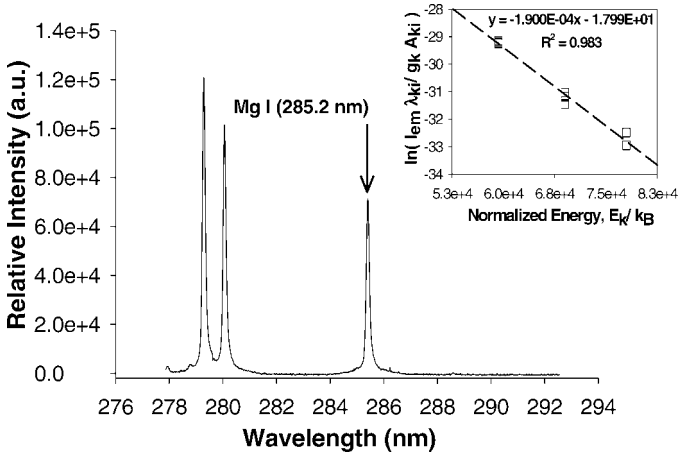

FIG. 10. Spectral signature of the Mg I (285.2 nm) transition line at a gate delay of 10 μs collected from breakdown of LAA powders. (**Inset**) The corresponding linear Boltzmann plot (regression coefficient of $R^2 \sim 0.983$) with Mg I transition lines (listed in Table II for LAA analysis) used for the calculation of $T_{exc} = -1/\text{Slope} = 5263 \pm 284$ K at delay time = 10 μs.

Mg I lines collected. Furthermore, the plasma excitation temperatures, T_{exc} at respective time delays of 3.5 μs and 10 μs were estimated from the linear Boltzmann plots of the eight strong transition lines of Mg I listed in Table II and also identified in our earlier work[12] as lines spread over wide energy levels. The corresponding insets in Figs. 9 and 10 show the linear fits to the respective Boltzmann plots with regression coefficients of $R^2 \sim 0.84$ and 0.98 created at delay times of 3.5 μs and 10 μs, respectively. The plasma excitation temperatures, T_{exc} estimated from the slope of these linear fits ($-1/T_{exc}$) were found to be 6076 ± 1102 K and 5263 ± 284 K at gate delays of 3.5 μs and 10 μs, respectively. The spectral data for I_{em} extracted from C I and Mg I emission line data and T_{exc} calculated at the respective time delays are further used in Eq. 1 to determine the relative population densities of carbon and magnesium elemental species.

For normalizing all our relative species densities with an internal calibration standard, two different emission lines were

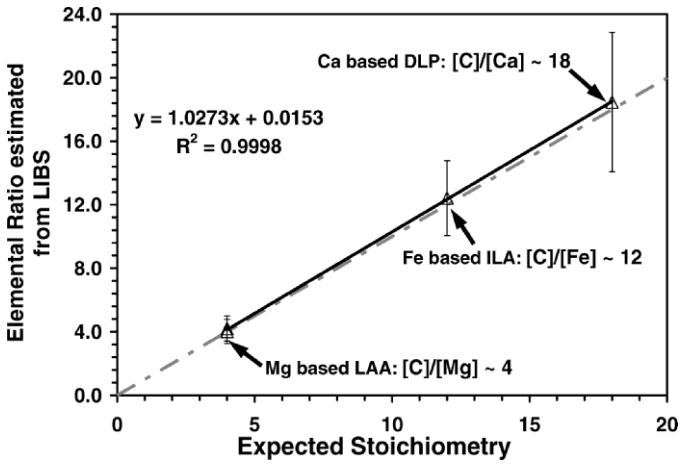

FIG. 11. Elemental ratios of [C]/[Mg], [C]/[Fe], and [C]/[Ca] estimated from LIBS analysis plotted as a function of the expected stoichiometric ratios based on their molecular formulae. The linear fit to the plot and the gray dash-dot line representing the ideal one-to-one correspondence indicate a good match between the two. The error bars indicate the statistical uncertainties at the 95% confidence interval.

TABLE III. Overall results indicating expected stoichiometric ratios and those estimated from LIBS analysis for [C]/[Mg], [C]/[Fe], and [C]/[Ca] in each of the cases of the three powdered drugs along with the respective uncertainties.

Drugs	Expected [C]/[X] ratio[a]	Estimated [C]/[X] ratio[a]
L-ascorbic acid (Mg based LAA)	4.00	4.02 ± 0.76[b]
	4.00	4.20 ± 0.79[c]
Iron L-Ascorbate (Fe based ILA)	12.00	12.42 ± 2.36
DL-Pantothenic Acid (Ca based DLP)	18.00	18.47 ± 4.39

[a] [X] refers to the trace elements Mg, Fe, and Ca in LAA, ILA, and DLP, respectively.
[b] Normalized by O I (777.2 nm) as explained in the text.
[c] Normalized by Mg I (518.4 nm) as explained in the text.

used in this case: (1) O I (777.2 nm), which we could use here since strong emission lines existed at both the gate delays of 3.5 μs and 10 μs, and (2) the Mg I (518.4 nm) transition line, which was used to validate the effectiveness of using one of the trace elements as the internal calibration standard. Our interest here was to verify whether the use of the Ca I (430.8 nm) emission line as the internal calibration standard in the earlier DLP analysis case was well justified. Since in this case we could get both the O I (777.2 nm) and Mg I (518.4 nm) lines at gate delays of 3.5 μs and 10 μs, we had the advantage of testing the uniformity of results that can be obtained by normalizing our species concentration data with both these lines individually. The species population densities of both $N_i^{\text{MgI(518.4nm)}}$ and $N_i^{\text{OI(777.2nm)}}$ calculated from the S/N ratio of the Mg I (518.4 nm) and O I (777.2 nm) emission lines collected at the respective gate delay times of 3.5 μs and 10 μs were individually used to normalize the species population densities N_i^{CI} and N_i^{MgI}, respectively, as shown in Eq. 2 earlier. In the two cases of normalization with $N_i^{\text{MgI(518.4nm)}}$ and $N_i^{\text{OI(777.2nm)}}$ carried out independently, the quantitative elemental ratio of [C]/[Mg] resulted in 4.02 ± 0.76 and 4.2 ± 0.79, which was in excellent agreement with the expected value of 4 from the molecular formula of LAA. All final uncertainties were calculated by propagating statistical errors through the uncertainties in S/N ratio and estimated plasma temperatures.

Finally, Fig. 11 shows the overall results obtained for the quantitative elemental composition analysis of all the aerosolized drugs by plotting the elemental ratios calculated from the LIBS spectral data against the expected stoichiometric elemental ratios of [C]/[Mg], [C]/[Fe], and [C]/[Ca] determined from the known molecular formula of each of the powdered drugs LAA, ILA, and DLP, respectively. The plot clearly indicates an excellent linear fit, with a slope of about 1.03, thereby indicating a one-to-one correspondence in the quantitative LIBS generated results and the expected values from the chemical formulae. To demonstrate the accuracy of our results, the dashed line in Fig. 11 indicates the expected ideal one-to-one correspondence between the values along the two axes. The error bars at each data point in Fig. 11 indicate the statistical uncertainties at the 95% confidence interval estimated from error propagation as described earlier. For ease of reference, overall results, along with the uncertainties from our experiments here, have been tabulated in Table III and Table IV. Table III indicates all the estimated elemental ratios and Table IV lays out the plasma excitation temperatures, T_{exc}, at 3.5 μs (for C I emission line analysis) and at 10, 13, and 29 μs (for Mg I, Fe I, and Ca I emission line analysis) for the three drugs LAA, ILA, and DLP.

TABLE IV. Plasma excitation temperatures, T_{exc}, and the respective uncertainties estimated from LIBS data analysis at different gate delay times corresponding to the optimal signals of C I, Mg I, Fe I, and Ca I lines for the three different powdered drugs under study.

	T_{exc} for carbon analysis		T_{exc} for trace element analysis	
Drugs	$T_{exc} \pm \Delta T_{exc}$ (K)	Gate delay (μs)	$T_{exc} \pm \Delta T_{exc}$ (K)	Gate delay (μs)
L-ascorbic acid (Mg based LAA)	6076 ± 1102	3.5	5263 ± 284	10 (for Mg I line)
Iron L-ascorbate (Fe based ILA)	6522 ± 872	3.5	6306 ± 849	13 (for Fe I line)
DL-pantothenic acid (Ca based DLP)	10374 ± 1877	3.5	7569 ± 1167	29 (for Ca I line)

We would like to point out the relatively large error bars associated with the ILA and DLP case studies, which also corresponds to the large uncertainties in the T_{exc} calculated in each of these cases. This reiterates our earlier discussion that a significant amount of statistical uncertainty in LIBS data might result from the plasma temperature calculations based on the linear Boltzmann plots. A large data set and the choice of a greater number of transition lines to create the Boltzmann plot could reduce these uncertainties.

CONCLUSION

The present study establishes LIBS as an effective analytical technique for on-line real-time analysis of aerosolized drugs. The results from the spectral data analysis developed on an internal calibration based quantitative LIBS methodology could accurately estimate the elemental ratio of carbon to trace elements such as Mg, Fe, and Ca within error limits for the three different powdered drugs LAA, ILA, and DLP, respectively. The elemental ratios of [C]/[Mg], [C]/[Fe], and [C]/[Ca] calculated from the LIBS spectral data analysis on each of the drugs LAA, ILA, and DLP were found to be 4.02 ± 0.76, 12.42 ± 2.36, and 18.47 ± 4.39, respectively, which were in excellent agreement with the expected stoichiometric ratios of 4, 12, and 18 based on their chemical formulae. We also conclude that although LIBS has enormous potential for on-line characterization of aerosolized drugs, it still has room for improvements since our results (as seen in Tables III and IV) indicate that it might involve a relatively large uncertainty arising mostly out of the statistical errors involved with plasma excitation temperature calculations that can vary significantly due to shot-to-shot laser energy variation or matrix initiated instabilities in the LIBS plasma. Finally, we would like to conclude that our results from the first-ever study on the application of LIBS for aerosolized drug analysis opens up future possibilities of exploring LIBS as a novel, fast, on-line diagnostic tool for quantitative analysis of pharmaceutical products in their manufacturing line.

ACKNOWLEDGMENTS

The work was supported by the Strategic Environmental Research and Development Program of the Department of Defense (D.M., M.D.C.). This work was partially funded by Powerscope Inc., Minneapolis, through a grant from NIH/National Heart Lung and Blood Institute, Grant # 1R43HL084831-01. Oak Ridge National Laboratory is managed by UT-Battelle, LLC, for the U.S. Dept. of Energy under contract DE-AC05-00OR22725. Appointment for D.M. to the ORNL Research Associates Program was jointly administered by ORNL and the Oak Ridge Institute for Science and Education.

1. D. W. Hahn and M. M. Lunden, Aerosol Sci. Technol. **33,** 30 (2000).
2. C. Aragon, J. A. Aguilera, and J. Campos, Appl. Spectrosc. **47,** 606 (1993).
3. M. Sabsabi and P. Cielo, Proc. Appl. Spectrosc. **49,** 499 (1995).
4. A. Gonzales, M. Ortiz, and J. Campos, Appl. Spectrosc. **49,** 1631 (1995).
5. R. E. Neuhauser, U. Panne, and R. Niessner, Anal. Chim. Acta **392,** 47 (1999).
6. M.-D. Cheng, Fuel Proc. Technol. **65–66,** 219 (2000).
7. R. E. Neuhauser, U. Panne, R. Niessner, and P. Wilbring, Fresnius' J. Anal. Chem. **364,** 720 (1999).
8. M. Martin and M. D. Cheng, Appl. Spectrosc. **54,** 1279 (2000).
9. D. Anglos, Appl. Spectrosc. **55,** 186A (2001).
10. J. E. Carranza, B. T. Fisher, G. D. Yoder, and D. W. Hahn, Spectrochim. Acta, Part B **56,** 851 (2001).
11. G. A. Lithgow, A. L. Robinson, and S. G. Buckley, Atmos. Environ. **38,** 3319 (2004).
12. D. Mukherjee and M. D. Cheng, J. Anal. At. Spectrom. **23,** 119 (2008).
13. J. D. Hybl, G. A. Lithgow, and S. G. Buckley, Appl. Spectrosc. **57,** 1207 (2003).
14. P. B. Dixon and D. W. Hahn, Anal. Chem. **77,** 631 (2005).
15. A. Gupta and P. B. Myrdal, J. Chromatogr., A **1033,** 101 (2004).
16. R. L. Green, M. D. Mowery, J. A. Good, J. P. Higgins, S. M. Arrivo, K. McColough, A. Mateos, and R. A. Reed, Appl. Spectrosc. **59,** 340 (2005).
17. D. J. Wargo and J. K. Drennen, J. Pharm. Biomed. **14,** 1415 (1996).
18. S. S. Sekulic, H. W. Ward, D. R. Brannegan, E. D. Stanley, C. L. Evans, S. T. Sciavolino, P. A. Hailey, and P. K. Aldridge, Anal. Chem. **68,** 509 (1996).
19. M. Andersson, S. Folestad, J. Gottfries, M. O. Johansson, M. Josefson, and K. G. Wahlund, Anal. Chem. **72,** 2099 (2000).
20. J. P. Higgins, S. M. Arrivo, G. Thurau, R. L. Green, W. Bowen, A. Lange, A. C. Templeton, D. L. Thomas, and R. A. Reed, Anal. Chem. **75,** 1777 (2003).
21. L. St-Onge, E. Kwong, M. Sabsabi, and E. B. Vadas, Spectrochim. Acta, Part B **57,** 1131 (2002).
22. M. D. Mowery, R. Sing, J. Kirsch, A. Razaghi, S. Bechard, and R. A. Reed, J. Pharm. Biomed. **28,** 935 (2002).
23. D. Heuser and D. S. Walker, J. Anal. Atom. Spectrom. **19,** 929 (2004).
24. D. Mukherjee, A. Rai, and M. R. Zachariah, J. Aerosol Sci. **37,** 1388 (2006).
25. Sigma-Aldrich Products Catalog Advanced Search website: http://www.sigmaaldrich.com/catalog/search/AdvancedSearchPage.
26. Y. Ralchenko, F.-C. Jou, D. E. Kelleher, A. E. Kramida, A. Musgrove, J. Reader, W. L. Wiese, and K. Olsen, *NIST Atomic Spectra Database* (version 3.1.1), [Online]. Available: HTU http://physics.nist.gov/asd3UTH (2007, March 29). National Institute of Standards and Technology, Gaithersburg, MD.
27. S. Yalcin, D. R. Crosley, G. P. Smith, and G. W. Faris, Appl. Phys. B **68,** 121 (1999).
28. Y.-I. Lee, K. Song, and J. Sneddon, *Laser Induced Breakdown Spectrometry* (Nova Science Publishers, Huntington, New York, 2000).
29. M. Sabsabi and J. Bussire, US Patent 5,781,289 (14 July 1998).
30. L. St-Onge, E. Kwong, M. Sabsabi, and E. B. Vadas, J. Pharm. Biomed. Anal. **36,** 277 (2004).
31. L. St-Onge, J.-F. Archambault, E. Kwong, M. Sabsabi, and E. B. Vadas, J. Pharm. Pharm. Sci. **8,** 272 (2005).